COMPEL - The international journal for computation and mathematics in electrical and electronic engineering

Adaptation in coupled problems
Christos Vokas, Manfred Kasper,

The current issue and full text archive of this journal is available at
www.emeraldinsight.com/0332-1649.htm

Adaptation in coupled problems

Christos Vokas and Manfred Kasper
Institute of Micro System Technology,
Hamburg University of Technology, Hamburg, Germany

Abstract

Purpose – The purpose of this paper is to address the formulation, implementation, and adaptation of closely coupled multi-physics problems with *h*- and *p*-adaptive finite element methods. A general formulation is chosen allowing for coupled problems of various types. Adaptation algorithms for *h*- and *p*-refinement are given.

Design/methodology/approach – A generic system of second-order differential equations is used, where the field of each individual problem is represented as an entry in the list of field variables. Specific problems are implemented by mapping material coefficients to the coefficients of the generic form. An example with four natures is investigated with close coupling between electric, mechanical and thermal fields. *h*- and *p*-refinement using a single mesh is considered, where the element order may differ for individual fields.

Findings – In coupled problems, the error in each single field is affected by approximation properties of all other field quantities. In order to allow for optimal convergence order in the number of degrees of freedom, the error contributions of all fields have to be considered. Separate error estimation in each field is needed especially in *h*-adaptation on a single mesh. Energy coupling coefficients were introduced to derive an adaptation criterion. Convergence analysis of *h*- and *p*-adaptation proves the feasibility of the approach.

Originality/value – Piezopyroelectricity considers thermal effects in high-frequency piezoelectric materials, which is a coupled problem of four natures. The paper introduces an adaptation criterion for such complicated coupled problems and proves feasibility.

Keywords Physics, Meshes, Problem solving, Finite element analysis, Error analysis

Paper type Research paper

Introduction

Coupled, multi-physics problems are ubiquitous in engineering applications and a wide variety of problems has been considered. Exemplarily, we mention fluid-structure interaction (Bathe and Zhang, 2009), coupling between magnetic field, mechanical deformation, and acoustic radiation (van Riesen and Hameyer, 2006), magnetic and thermal fields (Driesen *et al.*, 2002) or the coupling between electrostatic potential, charge carrier concentrations and carrier temperatures in highly nonlinear semiconductor devices (Chen and Liu, 2003). These examples show that problem formulation and numerical treatment are commonly problem specific. Publications on general and common principles in the numerical treatment of coupled problems are rare. In Michopoulos *et al.* (2005), modeling and simulation of multi-physics problems has been considered by distinguishing multi-field, multi-domain and multi-scale procedures, however with little emphasis on numerical or finite element aspects. Generally, weak and strong coupling have to be differentiated, thus leading to either a staggered or iterative solution procedure, or the requirement of simultaneous solution. Cross *et al.* (2007)

COMPEL: The International Journal for Computation and Mathematics in Electrical and Electronic Engineering
Vol. 29 No. 6, 2010
pp. 1626-1641

0332-1649
DOI 10.1108/03321641011078698

consider the modeling approach of closely coupled multi-physics problems using a generic model and a unified computational procedure, which allows for various physical phenomena like fluid flow, heat transfer, chemical reaction and electro-magnetics with special emphasis on multi-scale problems.

We here are interested in error control and adaptive methods in the case of strong coupling. While error estimation and mesh adaptation (Mackerle, 2001) is well established for single problems, only a few attempts have been made towards adaptive methods for coupled field problems. In most cases where adaptation is considered for multi-physics problems, the mesh is adapted to requirements of only one of the considered fields (Bathe and Zhang, 2009) and error indicators are derived in a heuristic way on the basis of field gradients (Chen and Liu, 2003).

Solin *et al.* (2010b) consider multi-mesh adaptation of the linear thermoelastic problem, where the thermal problem is independent of the mechanical stress distribution, i.e. the problem can be solved as a staggered problem. In their approach, individual meshes for the two displacements and the temperature are used and residuals are computed in the energy norm. We here consider *h*- and *p*-adaptation on a single mesh, i.e. *h*-refinement affects all fields simultaneously; however, the polynomial order may differ between the coupled field quantities.

One main idea behind our work is to create a mathematical framework that allows for the fast implementation of new coupled physics modes without having to do further extensive coding each time (Vokas and Kasper, 2008). For this reason, the general coupled-field partial differential equation (PDE) (equation (1)) was implemented in PolyDE (Kasper *et al.*, 2010):

$$\sum_{j=1}^{m} \left(-\nabla\left(\nu_{ij}\nabla_{u_j} + \gamma_{ij}u_j\right) + \beta_{ij}\nabla_{u_j} + \alpha_{ij}u_j\right) = f_i + \nabla_{g_i} \quad i \in [1, 2, \ldots, m] \tag{1}$$

In equation (1), each nature (or field quantity) is described by one PDE and in every PDE all the coupling effects resulting from the interaction with the other field quantities can be included. We kept the formulation in equation (1) as general as possible and map specific coupled problems by appropriately equating the coefficients α, β, γ, ν to the corresponding material coefficients. In this respect, the approach differs from implementations for solving specific problems. This paper presents algorithms for a coupled *p*-adaptation and a coupled *h*-adaptation technique. Both of these algorithms are applied on the same test problem and the adaptation results are presented later on in the text.

Piezoelectricity and piezopyroelectricity

Equation (1) can theoretically allow for an unlimited number of natures. We consider a physics mode called piezopyroelectricity which combines piezoelectricity and thermal effects. The four scalar field quantities are the mechanical displacements, one in *x*- and one in *y*-direction, electrostatics and temperature.

Piezoelectricity is formulated as in equation (2). There are three equations, the first two for the *x*- and *y*-mechanical displacements (u_x and u_y) and the third for the electric potential (Φ):

$$
\begin{aligned}
&-\operatorname{div}\left(\begin{bmatrix} C_{11} & C_{16} \\ C_{16} & C_{66} \end{bmatrix} \operatorname{grad}\ u_x\right) \\
&-\operatorname{div}\left(\begin{bmatrix} C_{16} & C_{12} \\ C_{66} & C_{26} \end{bmatrix} \operatorname{grad}\ u_y\right) \\
&-\operatorname{div}\left(\begin{bmatrix} e_{11} & e_{12} \\ e_{61} & e_{62} \end{bmatrix} \operatorname{grad}\ \Phi\right) = 0 \\
&-\operatorname{div}\left(\begin{bmatrix} C_{16} & C_{66} \\ C_{12} & C_{26} \end{bmatrix} \operatorname{grad}\ u_x\right) \\
&-\operatorname{div}\left(\begin{bmatrix} C_{66} & C_{26} \\ C_{26} & C_{22} \end{bmatrix} \operatorname{grad}\ u_y\right) \\
&-\operatorname{div}\left(\begin{bmatrix} e_{61} & e_{62} \\ e_{21} & e_{22} \end{bmatrix} \operatorname{grad}\ \Phi\right) = 0 \\
&-\operatorname{div}\left(\begin{bmatrix} e_{11} & e_{61} \\ e_{12} & e_{62} \end{bmatrix} \operatorname{grad}\ u_x\right) \\
&-\operatorname{div}\left(\begin{bmatrix} e_{61} & e_{21} \\ e_{62} & e_{22} \end{bmatrix} \operatorname{grad}\ u_y\right) \\
&-\operatorname{div}\left(\varepsilon_0 \begin{bmatrix} \varepsilon_{r,11} & \varepsilon_{r,12} \\ \varepsilon_{r,21} & \varepsilon_{r,22} \end{bmatrix} \operatorname{grad}\ \Phi\right) = 0
\end{aligned}
\tag{2}
$$

where:

- C are the entries of the rank-4 elasticity tensor.
- e are the entries of the rank-3 piezoelectric tensor.
- ε are the entries of the rank-2 permittivity tensor.

In some piezoelectric crystal classes of materials, an electric field on the *xy*-plane produces a stress in the *z*-direction. For this reason, simulating a 2D piezoelectric problem is not straightforward. The full 3D material property tensors have to be considered first and after performing a transformation (Nye, 1985) on them depending on the slice of the geometry that has to be simulated, the tensor entries that correspond to the *z*-direction can be dropped. In other words, the plane from the 3D geometry that has to be simulated is mapped onto a 2D *xy*-plane.

The piezopyroelectric physics mode is formulated as in equation (3):

$$
\begin{aligned}
&-\operatorname{div}\left(\begin{bmatrix} C_{11} & C_{16} \\ C_{16} & C_{66} \end{bmatrix} \operatorname{grad}\ u_x\right) - \operatorname{div}\left(\begin{bmatrix} C_{16} & C_{12} \\ C_{66} & C_{26} \end{bmatrix} \operatorname{grad}\ u_y\right) \\
&- \operatorname{div}\left(\begin{bmatrix} e_{11} & e_{12} \\ e_{61} & e_{62} \end{bmatrix} \operatorname{grad}\ \Phi\right) - \operatorname{div}\left(-\begin{bmatrix} M_{11} \\ M_{12} \end{bmatrix} T\right) - \rho\omega^2 u_x = 0 \\
&- \operatorname{div}\left(\begin{bmatrix} C_{16} & C_{66} \\ C_{12} & C_{26} \end{bmatrix} \operatorname{grad}\ u_x\right) - \operatorname{div}\left(\begin{bmatrix} C_{66} & C_{26} \\ C_{26} & C_{22} \end{bmatrix} \operatorname{grad}\ u_y\right) \\
&- \operatorname{div}\left(\begin{bmatrix} e_{61} & e_{62} \\ e_{21} & e_{22} \end{bmatrix} \operatorname{grad}\ \Phi\right) - \operatorname{div}\left(-\begin{bmatrix} M_{21} \\ M_{22} \end{bmatrix} T\right) - \rho\omega^2 u_y = 0 \\
&- \operatorname{div}\left(\begin{bmatrix} e_{11} & e_{61} \\ e_{12} & e_{62} \end{bmatrix} \operatorname{grad}\ u_x\right) - \operatorname{div}\left(\begin{bmatrix} e_{61} & e_{21} \\ e_{62} & e_{22} \end{bmatrix} \operatorname{grad}\ u_y\right) \\
&- \operatorname{div}\left(-\varepsilon_0 \begin{bmatrix} \varepsilon_{r,11} & \varepsilon_{r,12} \\ \varepsilon_{r,21} & \varepsilon_{r,22} \end{bmatrix} \operatorname{grad}\ \Phi\right) - \operatorname{div}\left(\begin{bmatrix} P_1 \\ P_2 \end{bmatrix} T\right) = 0 \\
&- \operatorname{div}\left(\begin{bmatrix} \lambda_{11} & \lambda_{12} \\ \lambda_{21} & \lambda_{22} \end{bmatrix} \operatorname{grad}\ T\right) - j\omega T_{ref} \begin{bmatrix} M_{11} & M_{12} \end{bmatrix} u_x \\
&- j\omega T_{ref} \begin{bmatrix} M_{21} & M_{22} \end{bmatrix} u_y + j\omega T_{ref} \begin{bmatrix} P_1 & P_2 \end{bmatrix} \Phi + j\omega\rho c_\rho T = 0
\end{aligned}
\tag{3}
$$

where:

- M are the entries of the rank-2 stress-temperature tensor.
- P are the entries of the rank-1 pyroelectric tensor.
- λ are the entries of the rank-2 thermal conductivity tensor.
- ρ is the density.
- ω is the angular frequency.
- c_p is the specific heat.

The number of equations in equation (3) is four. The fourth equation corresponds to the temperature field (T). Compared to equation (2), it can be seen that in the first equation of equation (3), there is a component linking the x-displacement to the temperature via the stress-temperature tensor M. The equation for the y-displacement also contains this same extra component. The third equation contains a term that links the electric potential to the temperature via the pyroelectric tensor P. The last (temperature) equation in equation (3) contains the reverse thermoelastic and pyroelectric effects, which come together with the time-harmonic term $j\omega$.

Error estimation

An error estimator gives an estimate for the error in a solution quantity and serves as a criterion for acceptance of the solution. An error indicator is used in the adaptive refinement and it should provide sufficient local information to control the adaptation process (Ainsworth and Oden, 2000). A major requirement is that the computation of an a-posteriori estimator should have reasonable cost. This is the main reason why we concentrate on explicit residual error indicators (Babuška and Strouboulis, 2001; Verfürth, 2005). The indicator serves to identify regions of the computational domain with insufficient precision.

Error estimators and indicators have been intensively studied in the case of uncoupled problems. Explicit element-wise residual estimators are especially simple to compute. In Petzoldt (2002), the Poisson equation in two and three dimensions with discontinuous coefficients is considered. The estimator is reliable and efficient. A similar result is reported in Bernardi and Verfürth (2000), which also extends to the case where ν is a tensor. The case of the reaction-diffusion or convection-diffusion equation requires some modification; however, the estimator is of similar type (Verfürth, 1998; Verfürth, 2005). For the Poisson equation and higher order elements in *hp*-adaptation, an error indicator is derived in Melenk and Wohlmuth (2001). The estimator in this case is reliable, i.e. it provides – up to a constant which is independent of the mesh size and polynomial degree – an upper bound of the error. In contrast to first-order elements, the lower bound however is p-dependent.

It is well known (Babuška and Strouboulis, 2001; Oden *et al.*, 2005) that the finite element method (FEM) in the case of the wave equations ($\alpha < 0$, $\nu > 0$) suffers from pollution error. In the presence of pollution, the finite element solution oscillates around a shifted solution, because wavelength is not correctly represented. With the pollution, an additional error term appears, which is independent of the interpolation error, thus it cannot be estimated by a residual error estimator. Despite the lack of a rigorous proof, explicit and implicit residual estimators are used in Oden *et al.* (2005), which is reasonable under a restriction of mesh size.

In the case of coupled problems, error estimation and adaptation highly increases in complexity and publications on this topic are rare. Although residuals can be computed for each of the field quantities separately, a generalization of explicit estimators in a straightforward manner is not possible. Liszka *et al.* (1997) suggest to use an implicit error estimator based on a generalization of Bank and Weiser (1985). An embedded pair of FEM solutions with different orders ($p + 1$) and mesh size ($h/2$) is used in Solin *et al.* (2010a). This approach is quite safe, however largely increases the number of degrees of freedom. In order to capture coupling effects in the error estimation, we suggest a refinement indicator based on residuals and in the style of explicit estimators by use of coupling coefficients derived on the basis of element energies.

We start by computing the residual for each of the elements in each of the natures. This is done for the internal residual (4) of the element and for the external residual (5)-(7). Index i stands for the nature, index j runs from 1 up to the number of natures m so that the coupling effects are considered in the calculation of the residuals:

$$\mathrm{r}_{in,i(\mathrm{T})} = \sum_{j=1}^{m} \left(-\nabla(\nu_{ij}\nabla u_j + \gamma_{ij}u_j) + \beta_{ij}\nabla u_j + \alpha_{ij}u_j\right) - f_i - \nabla g_i \quad i \in [1, 2, \ldots, m] \quad (4)$$

$$\mathrm{r}_{ex,i(\mathrm{T})} = \sum_{j=1}^{m} \left([[\nu_{ij}\nabla u_j + \gamma_{ij}u_j]]\right) + [[g_i]] \quad \partial T \not\subset \partial\Omega \quad i \in [1, 2, \ldots, m] \quad (5)$$

$$r_{ex,i(\mathrm{T})} = \sum_{j=1}^{m} \left(\nu_{ij}\nabla u_j + \gamma_{ij}u_j\right)\cdot\mathbf{n} + g_i\cdot\mathbf{n} - (p_i + q_i u_i) \quad \partial\mathrm{T} \subset \partial\Omega_2 \quad i \in [1,2,\ldots,m] \tag{6}$$

$$r_{ex,i(\mathrm{T})} = 0 \quad \partial\mathrm{T} \subset \partial\Omega_1 \quad i \in [1,2,\ldots,m] \tag{7}$$

In equation (5), the external residual evaluates the difference of normal flux density from both sides of the interface. The square brackets denote the operation: $[[u]] = (u_{\mathrm{T}} - u_{\mathrm{T}'})\cdot\mathbf{n}$, where T, T′ refer to adjacent triangles. We use equation (5) for the edges of the element where a neighboring element exists except at boundary segments. This is indicated with: $\partial T \not\subset \partial\Omega$. For general Neumann boundary conditions, we use equation (6) and for Dirichlet boundary conditions the equation (7). The element-wise error estimator is calculated for element T and nature i by taking:

$$\eta^2_{\mathrm{T},i} = W_{\mathrm{in},i}\left|r_{\mathrm{in},i}\right|^2_{\mathrm{L}_2(\mathrm{T})} + W_{\mathrm{ex},i}\left|r_{\mathrm{ex},i}\right|^2_{\mathrm{L}_2(\partial\mathrm{T}\not\subset\partial\Omega)} + W_{\mathrm{b},i}\left|r_{\mathrm{ex},i}\right|^2_{\mathrm{L}_2(\partial\mathrm{T}\subset\partial\Omega_2)} \tag{8}$$

In equation (8), we take the L_2 norm of the internal and external residuals and multiply with the appropriate weights. The weights depend on triangle shape and area as well as the material coefficients.

Adaptation

Equation (8) works well with the *p*-adaptation algorithm that is described below; however, it does not work well with our coupled *h*-adaptation algorithm. The reason is that in *p*-adaptation the element order is adapted independently in each nature. On the other hand, in *h*-adaptation, only one mesh is used for all natures. There are no multiple meshes. Therefore, the decision on mesh refinement has to take into account the error of all natures simultaneously.

In *p*-adaptation, there are no problems arising from the fact that the energy-norm in different natures is measured in different units. In *h*-adaptation, this turned out to be a problem. When the energy-norm in one nature is arithmetically (without taking the units into account) much larger than the energy-norms in the other natures, then it dominates the adaptation process, since the elements are refined mostly according to the residual error estimates in the dominating nature.

To treat this problem, we introduce a refinement indicator given in equation (9), which replaces the error estimator (equation (8)) during the *h*-adaptation process. It corresponds to one element and one nature and is denoted by e. To the original error estimator η, the contributions of the element error estimators coming from all other natures are added. Every time, η is multiplied by a factor which normalizes the energy norm and reflects the coupling between different natures (index E indicates the use of energy norm). There is a distinction between non-coupling energies (not arising from the coupling effects) and coupling energies. A coupling energy is denoted with unequal i and j indices. The new normalized element refinement indicator can now serve as a criterion in deciding on which elements to refine (split into sub-elements) during the *h*-adaptation process:

$$e^2_{\mathrm{T},i} = \left\{ \eta^2_{\mathrm{T},i} + \sum_{j=1, j\neq \mathrm{i}}^{m} \left(\eta^2_{\mathrm{T},j} \frac{|u|^2_{\mathrm{E},ij(\mathrm{T})}}{|\mathrm{u}|^2_{\mathrm{E},jj(\mathrm{T})}} \right) \right\} \frac{1}{|\mathrm{u}|^2_{\mathrm{E},ii}} \tag{9}$$

The implemented coupled *p*-adaptation algorithm is described here:

(1) Do from 1 up to the number of adaptation steps:
   - do from 1 up to the number of natures:
     - sort residual vector (each entry corresponds to the residual of 1 element);
     - raise polynomial order of the worst (e.g. 5 percent) elements by 1;
     - raise polynomial order of a further ≈ 25 percent of the elements if their residual is above some critical limit set in *maxres*;
     - check if polynomial orders in neighboring elements differ by more than 1. If YES, increase the order in the lower order element so that the difference is not greater than 1; and
     - check if polynomial orders of the same element but different natures differ by more than 2. If YES, increase the order in all natures except the one with the highest order so that the difference is not greater than 2.
   - end of natures loop;
   - calculate the multi-nature error. This is the highest value of all nature errors; The individual nature error is calculated by taking: $\sqrt{sumres(nature)/sumref(nature)} \cdot 100\%$; and
   - if the desired adaptation error is smaller than the multi-nature error, exit the adaptation loop.
(2) end of adaptation steps loop.

The coupled *h*-adaptation algorithm is described in the following:

- Calculate the refinement indicator *e* for all elements and natures.
- For each element and since *e* is normalized, sum *e* over all natures.
- Now, there is only one refinement indicator vector where each entry corresponds to one element, sort this vector, place the most problematic elements first.
- Find *errmax*, the largest individual element error and *errmin*. The value in *errmin* is either equal to one tenth of *errmax* or equal to the error of the element with index given by (*number of elements*/18 + 1) in the sorted vector. The smallest of these two values is assigned to *errmin*.
- Look for the elements whose error value falls between *errmax* and *errmin* and refine them.

Results

A surface acoustic wave (SAW) sensor is a device whose operation is based on the piezoelectric effect. A sinusoidal alternating voltage is applied to one or more sets of electrodes and an acoustic wave is produced in the substrate of the device. The acoustic waves that propagate on the surface of the substrate are called SAWs. The geometry and electric field of the SAW model is shown in Figure 1. For this simulation, the width of the substrate is 200 μm whereas the height is 30 μm. The corresponding dimensions for the electrodes are 10 and 2 μm.

A sinusoidal voltage of 10 V in amplitude is applied at two of the electrodes whereas the other two are grounded. The frequency of the alternating input voltage is

190 MHz. The substrate material is Lithium Niobate (LiNbO3) and the electrode material is aluminium. The LiNbO3 plane that is simulated is the *YX*-plane and according to Wong (2002) the propagation velocity of the surface waves along this plane is approximately 3,800 m/s. In Figures 2 and 3, the *x*- and *y*-displacement field plots are shown.

It can be seen from Figures 2 and 3 that the wavelength of the surface waves is 20 μm. Owing to the fact that in this type of problem wave reflections result at the boundaries of the geometry, Perfectly matched layers (PMLs) have been implemented in PolyDE in order to minimize these reflections (Mayer *et al.*, 2007; Michler *et al.*, 2007). There are three rectangular PML regions in the geometry. The first one damps the acoustic waves in the $+x$ direction, the second in the $-x$ and the third in the $-y$ direction. The damping is implemented in terms of the material parameters by making them complex inside the PML region.

The four-nature piezopyroelectric physics mode that is presented in this paper allows for the investigation of damping by thermoelastic dissipation simultaneously with the piezoelectric effect. The acoustic waves that are triggered by the alternating electrode voltage result in a temperature gradient. This temperature gradient is shown in Figure 4. It can be seen that at the regions of greater mechanical displacement – this is the surface of the substrate where the surface waves propagate – the temperature gradient is higher.

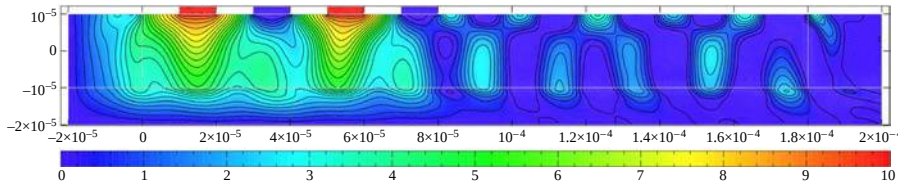

Note: Solution obtained with the piezopyroelectric physics mode

Figure 1.
Electric potential field plot of the SAW sensor

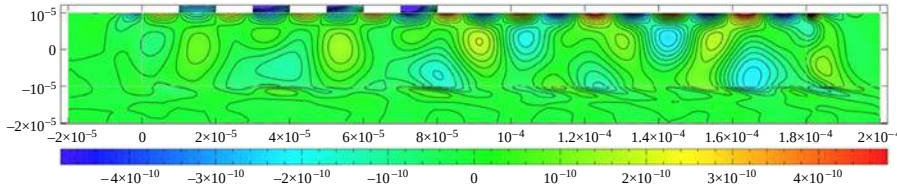

Note: Solution obtained with the piezopyroelectric physics mode

Figure 2.
X-displacement field plot of the SAW sensor

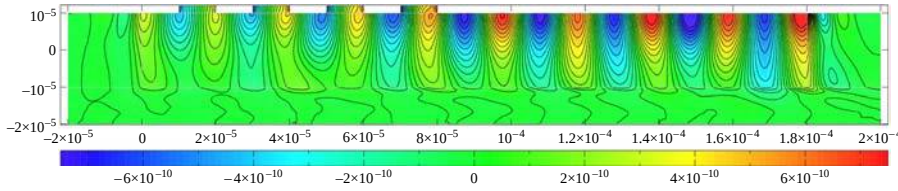

Note: Solution obtained with the piezopyroelectric physics mode

Figure 3.
Y-displacement field plot of the SAW sensor

The *h*-adaptation algorithm presented in the paper has been tested on the piezopyroelectric physics mode. We start with the coarse mesh shown in Figure 5. The element order is uniformly set to order 1, 2 or 3 and this means that it is not adapted during the *h*-adaptation process.

Figure 6 shows the resulting mesh after six *h*-adaptation steps. It is clear from Figure 6 that apart from the mesh refinement that is seen at the electrode corners due to the presence of singularities there, the PML regions become highly refined at internal boundaries. This can be due to the fact that damping in the PML region is not performed in a progressive manner but in an immediate manner. This means that at the interface between the LiNbO3 substrate and the LiNbO3-PML the material parameters change to complex values. Additionally, there is a refinement on the surface of the LiNbO3 substrate where the SAWs propagate.

The results from the application of the *h*-adaptation algorithm on this problem are shown in Figures 7-10. The plotted error indicator in these three graphs is given by equation (10):

$$R_i = \sqrt{\frac{\sum_{\mathrm{T}} \eta_{\mathrm{T},i}^2}{\sum_{j=1}^{m} \|u\|_{\mathrm{E},ij}^2}} \tag{10}$$

In equation (10), the sum of the error estimators for all elements in nature i, is normalized with respect to the energy content in the same nature. This is done because in a wave-propagation problem, the energy content changes when the mesh is changed during the adaptation process. If the error estimator is not normalized with respect to the energy then it will appear that there is no reduction in error during some adaptation steps and this is not true.

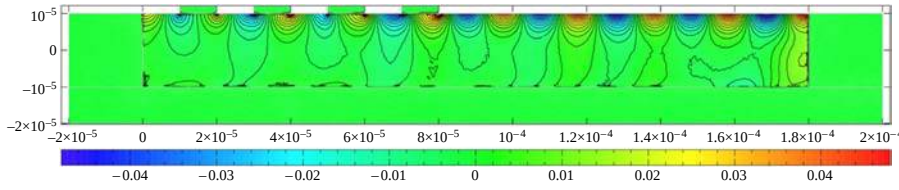

Figure 4.
Temperature field plot of the SAW sensor

Note: Solution obtained with the piezopyroelectric physics mode

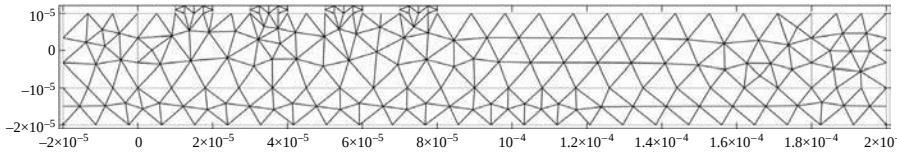

Figure 5.
Starting coarse mesh for the *h*-adaptation process

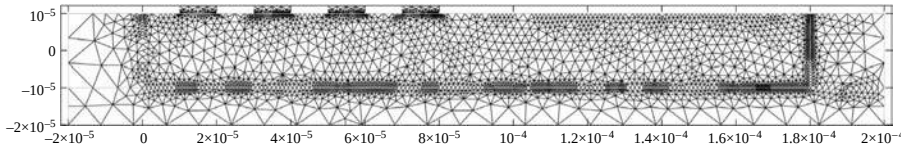

Figure 6.
Resulting mesh after six *h*-adaptation steps

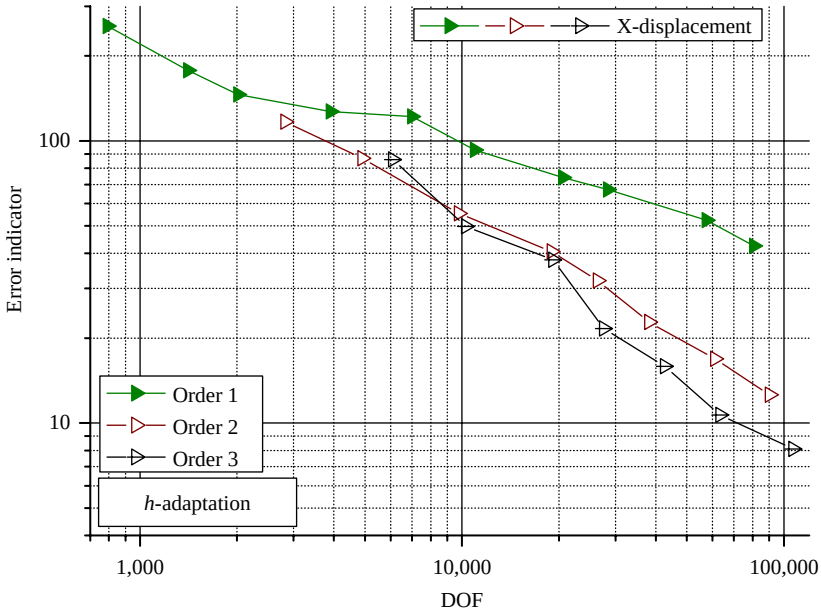

Figure 7.
X-displacement error indicator given by equation (10), plotted against number of degrees of freedom, with *h*-adaptation and for uniform element orders of 1, 2 and 3

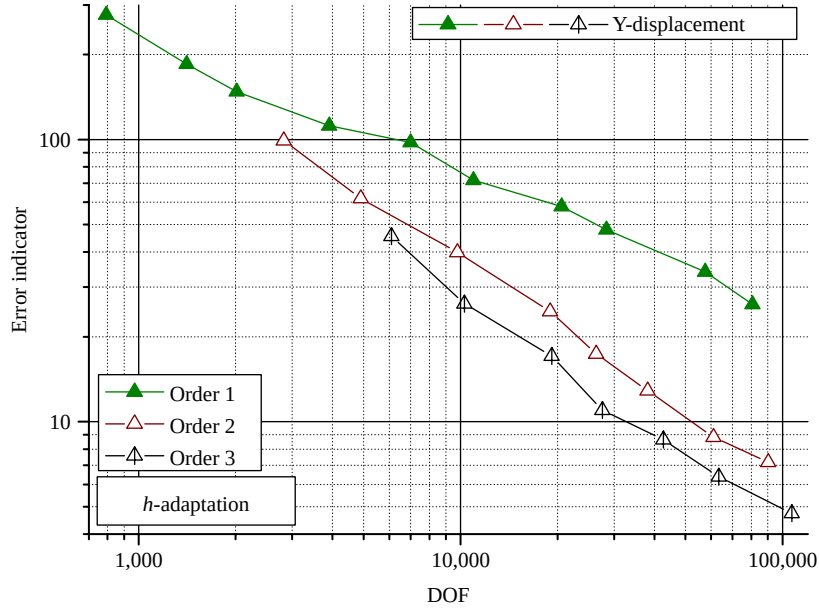

Figure 8.
Y-displacement error indicator given by equation (10), plotted against number of degrees of freedom, with *h*-adaptation and for uniform element orders of 1, 2 and 3

The *p*-adaptation algorithm has also been tested on this problem. The results are shown in Figures 11-13. Both the element-wise error estimator given by equation (8) and the refinement indicator (primarily, designed for the *h*-adaptation process) given by equation (9) were used as the adaptation criterion during the process.

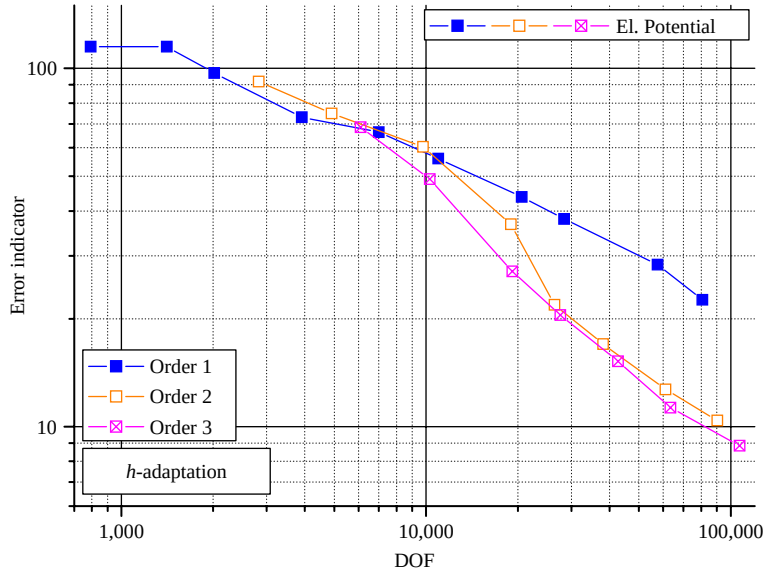

Figure 9.
Electric potential error indicator given by equation (10), plotted against number of degrees of freedom, with *h*-adaptation and for uniform element orders of 1, 2 and 3

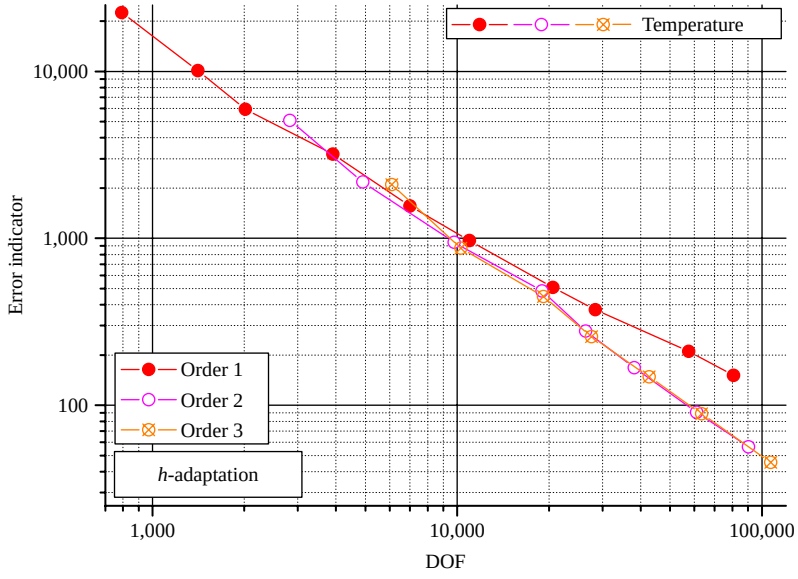

Figure 10.
Temperature error indicator given by equation (10), plotted against number of degrees of freedom, with *h*-adaptation and for uniform element orders of 1, 2 and 3

It is visible that the results obtained with equation (8) are slightly better. After approximately 30,000 DOF, the *p*-adaptation process enters a saturation phase and this is due to singularities in the problem.

Figures 14-17 show the resulting element order after ten adaptation steps for all natures of the piezopyroelectric problem in the following order (X-displacement,

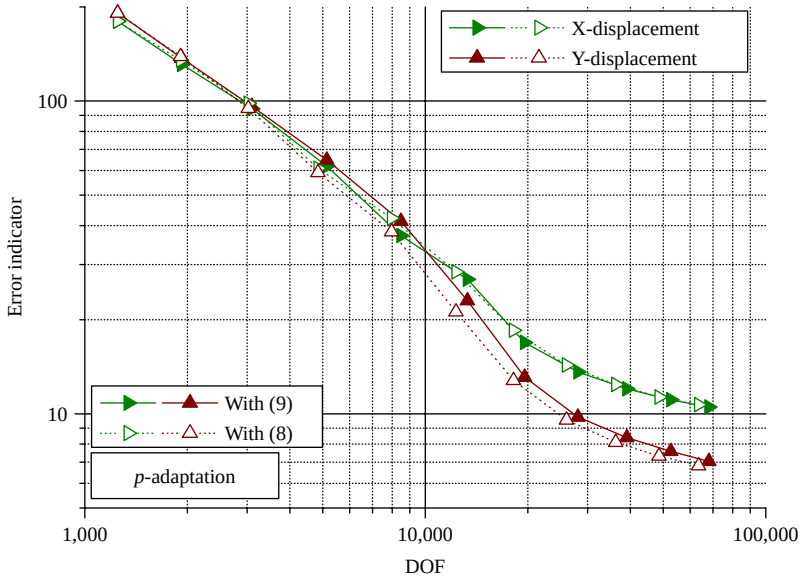

Figure 11.
X- and Y-displacement error indicators plotted against number of degrees of freedom, with *p*-adaptation and by using both the refinement indicator (equation (9)) and the error estimator (equation (8))

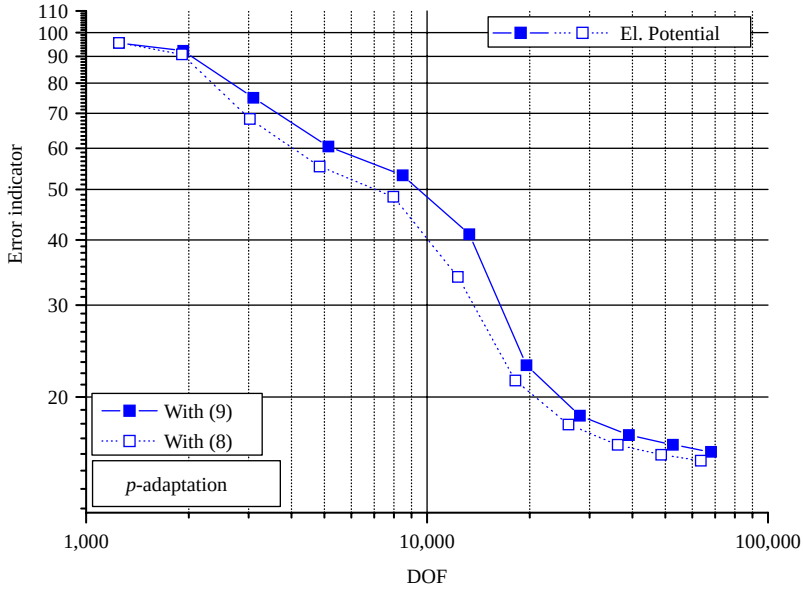

Figure 12.
Electric potential error indicator plotted against number of degrees of freedom, with *p*-adaptation and by using both the refinement indicator (equation (9)) and the error estimator (equation (8))

Y-displacement, electric potential, temperature). These plot were obtained using equation (9) as the adaptation criterion.

Figures 18-21 show the same plots as Figures 14-17 do, but this time using equation (8). We see a high element order at the corners of the electrodes and as well at

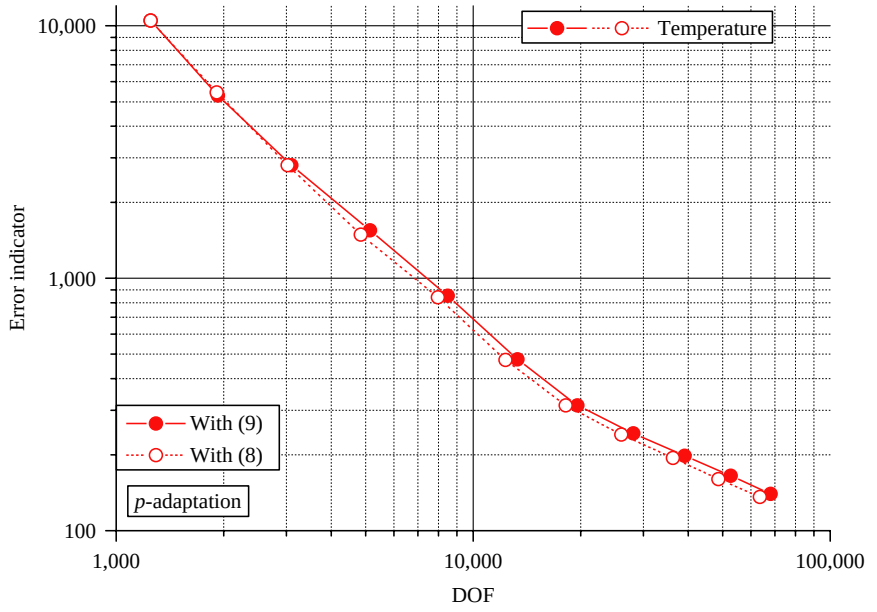

Figure 13.
Temperature error indicator plotted against number of degrees of freedom, with *p*-adaptation and by using both the refinement indicator (equation (9)) and the error estimator (equation (8))

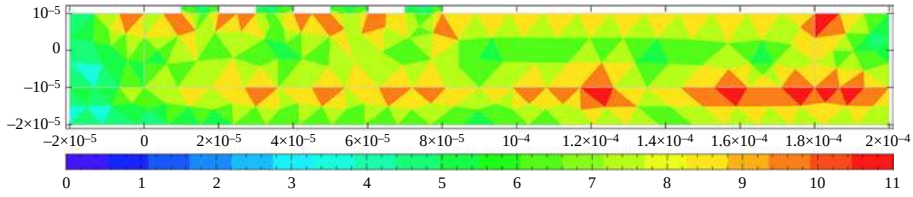

Figure 14.
Resulting element order for the X-displacement nature after ten *p*-adaptation steps using the refinement indicator of equation (9)

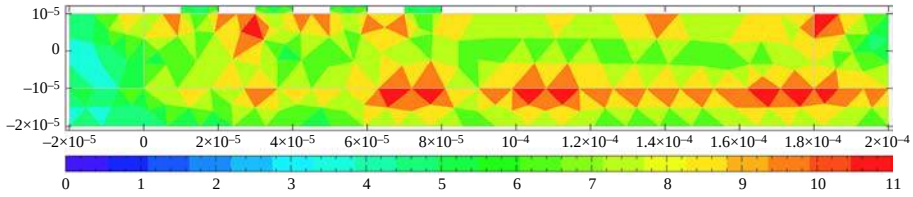

Figure 15.
Resulting element order for the Y-displacement nature after ten *p*-adaptation steps using the refinement indicator of equation (9)

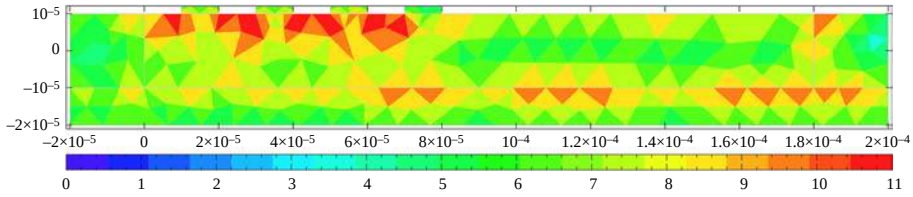

Figure 16.
Resulting element order for the electric potential after 10 *p*-adaptation steps using the refinement indicator of equation (9)

the PML boundaries. The error at the PML boundaries seems to be dominating the adaptation process in both cases with equations (9) and (8).

Conclusion

Convergence curves reflect the expected behavior and expected convergence rate, with slight deviations at higher order elements. Results indicate that adaptation of coupled problems with optimal convergence rate is possible using simple explicit error estimators.

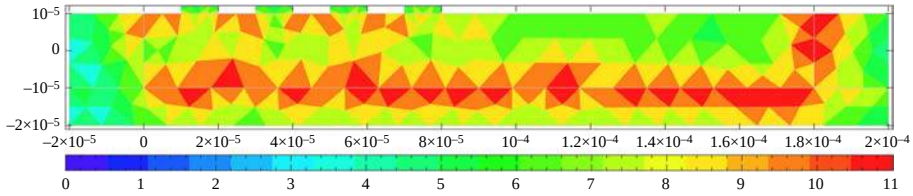

Figure 17.
Resulting element order for the temperature after ten *p*-adaptation steps using the refinement indicator of equation (9)

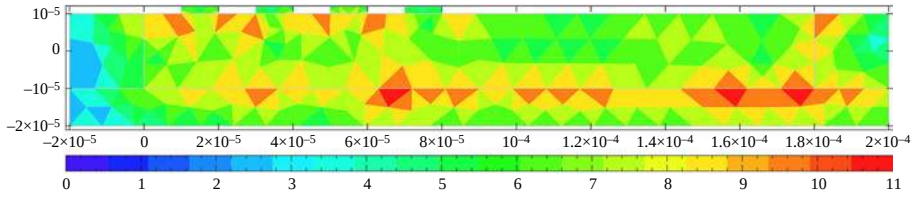

Figure 18.
Resulting element order for the X-displacement nature after ten *p*-adaptation steps using the error estimator of equation (8)

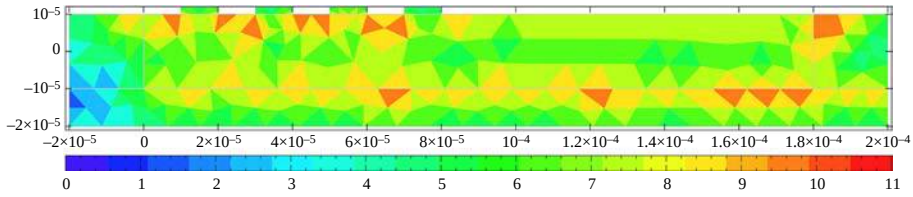

Figure 19.
Resulting element order for the Y-displacement nature after ten *p*-adaptation steps using the error estimator of equation (8)

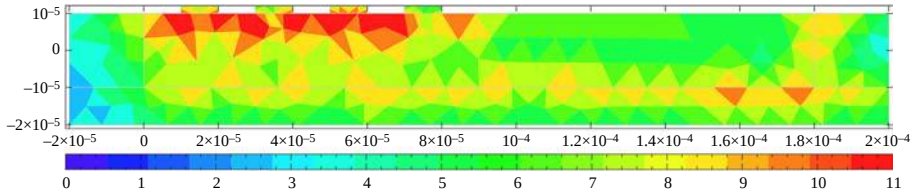

Figure 20.
Resulting element order for the electric potential after ten *p*-adaptation steps using the error estimator of equation (8)

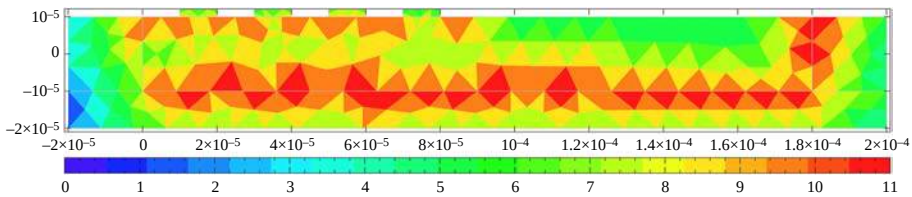

Figure 21.
Resulting element order for the temperature after ten *p*-adaptation steps using the error estimator of equation (8)

In *hp*-adaptation, additionally the decision about the refinement type has to be made. In this paper, the four-nature piezopyroelectric physics mode has been presented. Multi-nature *h*- and *p*-adaptation algorithms have been tested on this problem with comparable results. Self-adaptivity is a mandatory characteristic of reliable and efficient modern discretization methods.

References

Ainsworth, M. and Oden, J.T. (2000), *A Posteriori Error Estimation in Finite Element Analysis*, Wiley, New York, NY.

Babuška, I. and Strouboulis, T. (2001), *The Finite Element Method and Its Reliability*, Oxford University Press, New York, NY.

Bank, R.E. and Weiser, A. (1985), "Some a posteriori error estimators for elliptic partial differential equations", *Math. Computation*, Vol. 44, pp. 283-301.

Bathe, K.J. and Zhang, H. (2009), "A mesh adaptivity procedure for CFD and fluid-structure interactions", *Computers & Structures*, Vol. 87, pp. 604-17.

Bernardi, C. and Verfürth, R. (2000), "Adaptive finite element methods for elliptic equations with non-smooth coefficients", *Numerische Mathematik*, Vol. 85, pp. 579-608.

Chen, R.C. and Liu, J.L. (2003), "An iterative method for adaptive finite element solutions of an energy transport model of semiconductor devices", *Journal of Computational Physics*, Vol. 189 No. 2, pp. 579-606.

Cross, M., Croft, T.N., Slone, A.K., Williams, A.J., Christakis, N., Patel, M.K., Bailey, C. and Pericleous, K. (2007), "Computational modelling of multi-physics and multi-scale processes in parallel", *International Journal for Computational Methods in Engineering Science and Mechanics*, Vol. 8 No. 2, pp. 63-74.

Driesen, J., Belmans, R. and Hameyer, K. (2002), "Computation algorithms for efficient coupled electromagnetic-thermal device simulation", *IEE Proceedings-science, Measurement & Technology*, Vol. 149, pp. 67-72.

Kasper, M., Rahman, R.A. and Vokas, C. (2010), "sourceforge.net PolyDE", available at: http://sourceforge.net/projects/polyde-fem/ (accessed 10 April 2010).

Liszka, T., Tworzydlo, W., Bass, J., Sharma, S., Westermann, T. and Yavari, B. (1997), "ProPHLEX – an hp-adaptive finite element kernel for solving coupled systems of partial differential equations in computational mechanics", *Computer Methods in Applied Mechanics and Engineering*, Vol. 150 No. 4, pp. 251-71.

Mackerle, J. (2001), "Error estimates and adaptive finite element methods: a bibliography (1990-2000)", *Engineering Computations: International Journal for Computer-Aided Engineering*, Vol. 18 Nos 5/6, pp. 802-914.

Mayer, M., Zaglmayr, S., Wagner, K. and Schöberl, J. (2007), "Perfectly matched layer finite element simulation of parasitic acoustic wave radiation in microacoustic devices", paper presented at the IEEE Ultrasonics Symposium, New York, NY.

Melenk, J.M. and Wohlmuth, B.I. (2001), "On residual-based a posteriori error estimation in hp-FEM", *Advances in Computational Mathematics*, Vol. 15, pp. 311-31.

Michler, C., Demkowicz, L., Kurtz, J. and Pardo, D. (2007), "Improving the performance of perfectly matched layers by means of hp-adaptivity", *Numerical Methods for Partial Differential Equations*, Vol. 23 No. 4, pp. 832-58.

Michopoulos, J.G., Farhat, C. and Fish, J. (2005), "Modeling and simulation of multiphysics systems", *Journal of Computing and Information Science in Engineering*, Vol. 5 No. 3, pp. 198-213.

Nye, J.F. (1985), *Physical Properties of Crystals*, Oxford University Press, New York, NY.

Oden, J.T., Prudhomme, S. and Demkowicz, L. (2005), "A posteriori error estimation for acoustic wave propagation problems", *Archives of Computational Methods in Engineering*, Vol. 12 No. 4, pp. 343-89.

Petzoldt, M. (2002), "A posteriori error estimators for elliptic equations with discontinuous coefficients", *Advances in Computational Mathematics*, Vol. 16, pp. 47-75.

Solin, P., Andrs, D. and Cerveny, J. (2010a), "PDE-independent adaptive hp-FEM based on hierarchic extension of finite element spaces", *Journal of Computational and Applied Mathematics*, Vol. 233 No. 12, pp. 3086-94, available at: www.sciencedirect.com/science?_ob=ArticleURL&_udi=B6TYH-4WDNKS8-1&_user=506065&_coverDate=04%2F15%2F2010&_rdoc=1&_fmt=high&_orig=search&_sort=d&_docanchor=&view=c&_searchStrId=1294728572&_rerunOrigin=google&_acct=C000025031&_version=1&_urlVersion=0&_userid=506065&md5=1be5e96a9d3594044d10f97c6698bca1-aff2

Solin, P., Cerveny, J., Dubcova, L. and Andrs, D. (2010b), "Monolithic discretization of linear thermoelasticity problems via adaptive multimesh hp-FEM", *Journal of Computational and Applied Mathematics*, Vol. 234 No. 7, pp. 2350-7.

van Riesen, D. and Hameyer, K. (2006), "Coupled electromagnetic, structural-dynamic, and acoustic simulation of an induction furnace", *IEEE Transactions on Magnetics*, Vol. 42 No. 4, pp. 1019-22.

Verfürth, R. (1998), "Robust a posteriori error estimators for a singularly perturbed reaction-diffusion equation", *Numerische Mathematik*, Vol. 78, pp. 479-93.

Verfürth, R. (2005), "Robust a posteriori error estimates for stationary convection-diffusion equations", *SIAM Journal on Numerical Analysis*, Vol. 43, pp. 1766-82.

Vokas, C. and Kasper, M. (2008), "FEM implementation and p-adaptation of coupled problems", *Proceedings of the 13th IGTE Symposium in Graz, Austria*.

Wong, K.K. (2002), *Properties of Lithium Niobate*, The Institution of Electrical Engineers, London.

About the authors

Christos Vokas was born in Kavala, Greece in 1982. He graduated with an MEng degree in Computing and Communication Systems from Manchester (University of Manchester Institute of Science and Technology) in 2005. He then completed an MSc in Microelectronics and Microsystems in Hamburg (Technische Universität Hamburg-Harburg (TUHH)) in 2008. He is currently a PhD student at the Institute of Micro System Technology of The TUHH. His research area is concerned with the FEM, in particular adaptive techniques and coupled problems. Christos Vokas is the corresponding author and can be contacted at: vokas@tu-harburg.de

Manfred Kasper received the Dipl.-Ing. degree from the Darmstadt University of Technology in 1982 and the Dr-Ing. degree in Electrical Engineering from Technische Universität Berlin, Germany in 1990. From 1989 to 1994, he was at the Berlin Center of Advanced Packaging and from 1994 to 1996 the Fraunhofer Institute for Reliability and Microintegration in Berlin. Since 1996, he is with the Hamburg University of Technology, where he is a Professor in the Electrical Engineering Department. His main fields of interest include microsystem modelling and design with emphasis on FEMs.